Journal of
Ceramic Science
and Technology

J. Ceram. Sci. Tech., 07 [04] 313-322 (2016)
DOI: 10.4416/JCST2016-00036
available online at: http://www.ceramic-science.com

Low-Temperature Degradation Behaviour and Mechanical Properties of a 3Y-TZP Manufactured from Detonation-Synthesized Powder

F. Kern*, V. Lindner, R. Gadow

University of Stuttgart, IFKB

received May 12, 2016; received in revised form July 15, 2016; accepted August 18, 2016

Abstract

In recent years, yttria-stabilized zirconia Y-TZP has attracted considerable interest in the field of dental restoration. However, the state-of-the-art Y-TZP materials made from coprecipitated powders only just comply with the current standard in terms of fracture resistance and grain size. In this study a new nanoscale starting powder produced with detonation synthesis was applied to produce a fully dense specimen by means of hot pressing in the sintering temperature range between 1250 – 1500 °C. Mechanical properties, microstructure and phase composition were studied. Low-temperature degradation behavior was quantified in an accelerated ageing test in a saturated water vapor at 134 °C. Between sintering temperatures of 1300 °C and1400 °C, the materials obtained show a combination of high strength > 1400 MPa, toughness of 6 MPa√m and fine grain size < 320 nm and thus fulfill the requirements of the dental standard EN ISO 6872. Ageing resistance was high. After nucleation of the monoclinic content, the materials exhibited zero-order growth kinetics and retained > 90 % tetragonal phase up to ageing times of 10 h ≈ 35 years *in vivo*.

Keywords: Zirconia, mechanical properties, phase composition, microstructure, low-temperature degradation

I. Introduction

Partially stabilized zirconia ceramics derive their excellent mechanical properties, i.e. strength and fracture resistance, from an effect called "transformation toughening". With the addition of stabilizer oxides such as yttria, ceria or magnesia, the tetragonal phase remains metastable after sintering. Partially stabilized zirconia exists in two basic types: PSZ-type material such as Mg-PSZ, here the tetragonal precipitates are contained in a cubic matrix and TZP-type such as Y-TZP, here the material is very fine-grained and predominantly tetragonal. Exposed to mechanical stress such as at a loaded crack tip, the metastable tetragonal phase transforms martensitically (athermal, diffusionless and with the speed of sound in the material) to thermodynamically stable monoclinic phase. As this transformation is associated with dilatation (~ 5 vol%) and shear, the proceeding crack is put under compressive stress so that the stress intensity at the crack tip is lowered [1,2]. In Y-TZP the incorporation of aliovalent Y^{3+} into the zirconia lattice leads to the formation of oxygen vacancies to retain charge neutrality. Oversized dopants such as Y^{3+} favor an eightfold coordination, the oxygen vacancies are associated with the Zr^{4+} cations [3]. Y-TZP typically stabilized with ~ 3 mol% Y_2O_3 forms a tetragonal/cubic (80/20) solid solution [4]. Owing to the high transformation stresses that would exceed the material strength (which is determined by the size of flaws), standard 3Y-TZP typically has very high flexural strength of > 1000 MPa and moderate fracture resistance of ~ 5 MPa√m [5]. The state-of-the-art procedure to synthesize Y-TZP powders is coprecipitation, which involves zirconia and yttria being simultaneously precipitated from inorganic precursors. This leads to powders with a homogeneous stabilizer distribution at the atomic level. An alternative powder technological route to produce Y-TZP powders is coating zirconia with yttria in a wet chemical process or intensive comilling of both constituents, leading to higher fracture resistance and improved low-temperature degradation stability [6–9]. However, this type of powder is not commercially available. The main drawback in using Y-TZP in moist environments such as inside the human body is its tendency to low-temperature degradation (LTD). LTD is induced by polar molecules, typically water, which dissociate and oxygen-containing species occupy the oxygen vacancies in the lattice [10]. As a consequence of that, the tetragonal phase is destabilized and transforms to monoclinic without any external mechanical stress. The volume expansion of the transformed domains puts the surface of components under compressive stress and leads to opening up of grain boundaries, thereby facilitating the interpenetration of fluid into the bulk of the material [11]. Problems with LTD and *in vivo* failure of ceramic hip joints were the main reason for banning Y-TZP from applications in arthroplasty [12]. The kinetics of LTD is typically described a nucleation and growth model according to Mehl, Avrami and Johnson [13]. Comprehensive review articles on LTD have been published by Chevalier *et al.* [14–15].

The emulsion detonation process (EDS) for Y-TZP powder synthesis starts with a water in oil emulsion in which

* Corresponding author: frank.kern@ifkb.uni-stuttgart.de

the aqueous constituent acts as the oxidizer and the oil-based constituent as combustible fuel. The powder precursor is homogeneously dissolved in this emulsion. During detonation of the mixture, high temperatures up to 1400 °C and high pressures up to 10 GPa lead to formation of ultrafine powders that are subsequently quenched to retain small grain sizes and thus achieve high sinterability. A variation of the process also allows coating of nanoparticles with a second phase to obtain mixed oxides [16–19].

Y-TZP starting powders produced by means of EDS have become available recently, thus we aimed to investigate the mechanical properties and LTD characteristics of Y-TZP ceramics produced therefrom. Hot pressing was chosen to enable the production of fully dense materials –– from a limited amount of starting powder – over a wide sintering temperature range.

II. Experimental

The powder was a 3Y-TZP supplied by Innovnano, Portugal. The powder was manufactured by means of EDS using a patented process [20]. The as-synthesized agglomerated powder was characterized by means of XRD analysis (Bruker D8, Germany, Bragg-Brentano setup, CuKα-radiation) in respect of phase composition and primary crystallite size. In the 2theta range between 27°– 33° the areas and widths at half height of the three characteristic reflections of monoclinic (-111 and 111) as well as tetragonal (101) were determined. The phase composition was calculated using the Toraya calibration curve [21]. The crystallite sizes were estimated using the Scherrer formula [22]. The yttria content was determined with EDX (Leo, Cambridge, UK).

Samples were consolidated by hot pressing in vacuum (FCT Anlagenbau, Germany). The powder was filled into the boron-nitride-clad graphite die. The die was inserted into the press at 3 MPa pre-load and evacuated, then heating to 1150 °C proceeded at 30 K/min. At this temperature, the load was increased to 20 MPa for 10 min then heating to final temperature was performed at 30 K/min. Final temperatures were varied between 1250 °C and 1500 °C in 50-K increments to cover a wide range of sintering parameters, dwell was 1 h at 40 MPa. Two disks, each measuring 45 mm in diameter and 2.5 mm in thickness separated by a 10-mm graphite disk, were pressed at the same time, two extra disks were pressed at 1400 °C for ageing experiments. The disks were subsequently ground manually on both sides to remove the circumferential edge and the BN layer and then automatically lapped on both sides with 15-µm diamond suspension and polished with 15-, 6-, and 1-µm diamond suspension for 30 min in each case until a mirror-like surface was obtained (Struers Rotopol, Denmark). Elastic modulus E, Shear modulus G and Poisson's ratio ν were measured on whole polished disks by means of ultrasonic excitation (IMCE, Belgium). Density was determined on whole disks with the buoyancy method. The disks were then cut into bars of 4 mm in width for bending tests (ten samples) and fracture resistance tests (four samples for indentation strength in bending ISB, two for stable indentation crack growth in bending SIGB). The sides of bending bars were lapped and the edges were beveled. The remaining pieces were kept for Vickers hardness testing HV10 (Bareiss, Germany, load 98.1 N for 10 s) and XRD analysis. The bending strength was measured in a 4-pt setup (ten samples each; 20/10 mm inner/outer span, 0.5 mm/min, Zwick, Germany). Fracture resistance was determined with residual strength measurements (ISB) immediately after HV10 indentation on the tensile side (four samples each; 20/10 mm inner/outer span, 1.5 mm/min, Zwick, Germany) [23]. For the sake of completeness and comparability with many other publications, indentation fracture resistance based on direct crack length measurement was performed according to Niihara using the equation for Palmqvist cracks [24]. The resistance to subcritical crack growth was measured by means of stable indentation crack growth in bending (SIGB) according to a protocol explained by Dransmann and Benzaid [25,26]. For the SIGB tests the samples were indented with four HV10 indents with cracks parallel and perpendicular to the sides at a distance of 2 mm. The bars were then stored for two weeks to allow the cracks to grow to a stable extension. The area with the indents was placed on the tensile side within the inner span of the 4-pt test setup. Tests were carried out on 1–2 samples each; 20/10 mm inner/outer span at 2.5 mm/min. Samples were loaded starting from a strength value corresponding to 1/3 of the ISB residual strength and loaded successively at strength increments of 1/10 of ISB strength until fracture. After each loading/unloading cycle, the crack length was measured with the microscope of the hardness testing machine. The phase composition of the polished surface and of the straight fracture faces after ISB test was determined by means of XRD as described above for the powder [21]. Based on these data, the depth h of the transformation zones in the fracture faces was determined by means of XRD according to Kosmac [27]. The transformation toughness increments $\Delta K_{IC}{}^{T} = 1/(1\text{-}\nu)\cdot V_f \cdot E \cdot \sqrt{h} \cdot \varepsilon_T$ were calculated from measured data of E, ν, V_f and h according to McMeeking [28]. For the transformation strain ε_T a value of 0.05 was assumed. For the transformation efficiency X the literature value 0.27, i.e. largely dilatory transformation behavior, was chosen. The LTD resistance was measured in an accelerated ageing test in an autoclave at 134 °C in saturated water vapor (vapor pressure 3 bar). The phase composition of aged sample surfaces and the thickness of the layer of monoclinic zirconia were determined with XRD [27]. The values measured with the XRD method were cross-checked with layer thickness values determined by means of light microscopy (Leitz, Germany) and SEM (Leo Cambridge, UK) on polished cross-sections. The roughness of the aged surfaces was measured with a tactile method (Mahr, Germany) based on an average value of five lines of 5 mm in length. The topography of aged surfaces was qualitatively visualized with optical microscopy using differential interference contrast DIC. For determination of the microstructure of the ceramics, polished samples of each sintering temperature were thermally etched in hydrogen at 1200 °C for 10 min and subsequently studied by means of HRSEM (Zeiss Gemini, Germany). Grain sizes

were determined with the linear intercept method using Mendelson's correction factor [29].

III. Results

(1) Powder characteristics

The XRD pattern of the starting powder in the relevant 2theta range between 27 – 33° is shown in Fig. 1. The pattern observed is typical for a mixture of monoclinic and tetragonal zirconia; free yttria was not observed. The peak widths (2theta) for the three main peaks were measured as 0.374° ± 0.014° $(-111)_m$, 0.515° ± 0.014° $(101)_t$ and 0.507° ± 0.02° $(111)_m$. According to the Scherrer equation, this corresponds to crystallite sizes of 24 – 32 nm for the monoclinic and 24 nm for the tetragonal fraction [22]. Peak areas were integrated and a phase analysis according to Toraya was carried out [21]. The monoclinic fraction in the starting powder amounts to 59.5 ± 0.3 vol%. Compared to unstabilized zirconia nanopowder (Evonik VP-Ph, 68 vol% monoclinic, grain size 25 nm) analyzed in a previous publication, the tetragonal fraction is higher [30]. The yttria content determined by means of EDX in sintered samples was 2.85 ± 0.15 mol%, the composition of the powder is thus in the typical range for 3Y-TZP.

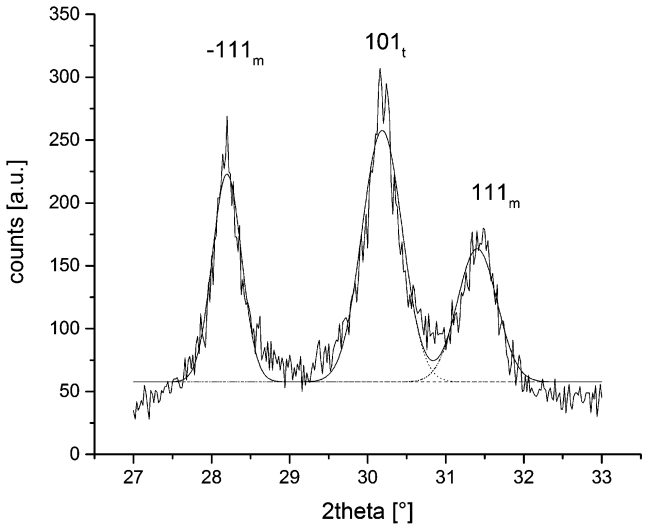

Fig. 1: XRD trace of the starting powder in the 2theta range between 27 – 33°, Fit of $(-111)_m$, $(101)_t$ and $(111)_m$ reflections.

(2) Microstructure

Fig. 2 shows the microstructure of materials sintered at 1300 °C, 1400 °C and 1500 °C at identical magnification (the scale bar is valid for all three images). The slightly corrugated structure is an artefact of the relatively gentle thermal etching process coupled with high-resolution SEM. What can be seen is the onset of recrystallization, revealing facets on the surface depending on the crystal orientation of the individual grains. In materials with larger grain size this rumpling is more pronounced than in fine-grain materials. The evolution of grain sizes with sintering temperatures is indicated in Fig. 3. Grain growth is very moderate up to a sintering temperature of 1400 °C. Here grain sizes reach a value of 320 ± 40 nm. Beyond this sintering temperature, grain growth is considerable and grain sizes reach 650 nm at 1500 °C. The largest grains reach sizes of ~ 1 µm, their surface is, however. not perfectly smooth, which together with their moderate size is an indication that they are not crystallized into the cubic phase system. The alumina content of the powder amounts to ~ 0.5 vol%, alumina grains have sizes of 200 – 300 nm and are homogeneously distributed in the zirconia matrix.

(3) Phase composition

Fig. 4 shows the monoclinic content in polished surfaces ($V_{m,\,polished}$) and the monoclinic content in fractured faces ($V_{m,\,fractured}$) of Y-TZP samples sintered at different temperatures. The monoclinic content in the polished surface decreases with rising sintering temperature from 2 vol% at 1250 °C to 0 vol% at 1350 °C. At higher sintering temperature no monoclinic can be quantified. The monoclinic in the fracture face slightly decreases from 6 vol% at 1250 °C to 5 vol% at 1350 °C. From 1400 °C upwards the monoclinic content in the fractured face starts to increase and reaches 11.5 vol% at 1500 °C. The accuracy of the measurement is in the range of 1 vol% absolute, thus changes within this range should not be overstressed. The transformability $V_f = V_{m,\,fractured} - V_{m,\,polished}$ rises from ~4 vol% at 1250 – 1350 °C to 11.5 vol% at 1500 °C. The thickness (h) of the transformation zone determined by means of XRD [27] ranges between 0.2 µm for the least to 0.65 µm for the most transformable materials. The low transformability also affects the transformation toughness increments ΔK_{IC}^{T}. ΔK_{IC}^{T} varies between 0.1 and 0.6 MPa$\sqrt{m}$ [28].

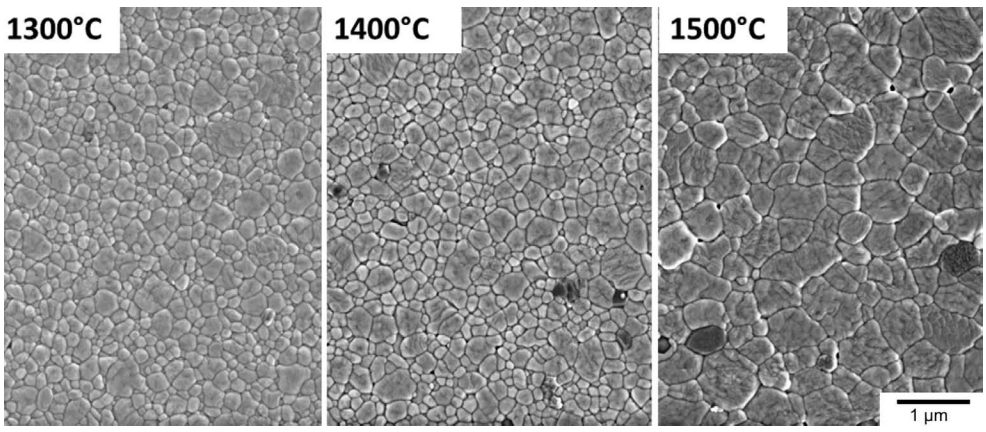

Fig. 2: SEM images of polished thermally etched Y-TZP samples sintered at 1300 °C, 1400 °C and 1500 °C.

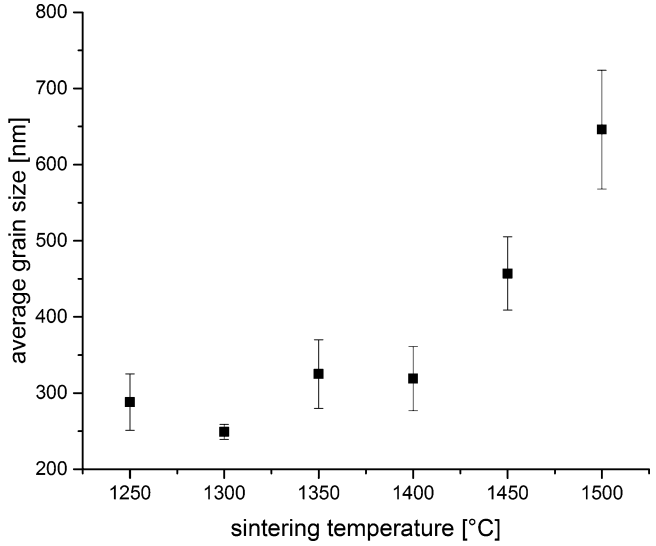

Fig. 3: Evolution of average grain sizes of Y-TZP with sintering temperature.

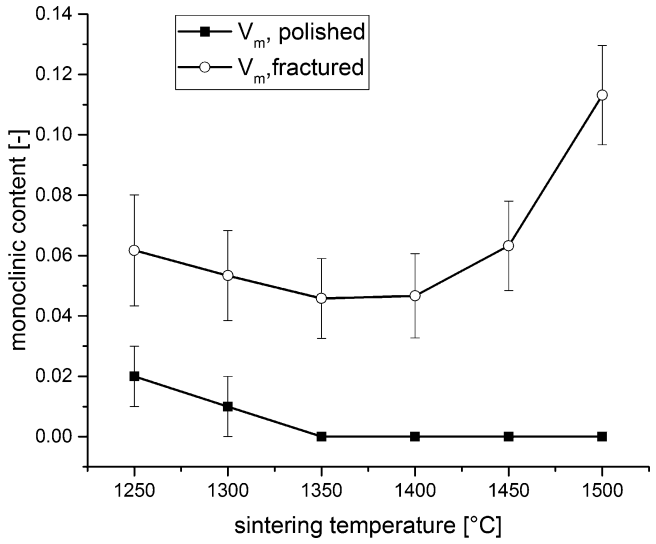

Fig. 4: Monoclinic content in polished surfaces ($V_{m,polished}$) and the monoclinic content in fracture faces ($V_{m,fractured}$) of Y-TZP samples sintered at different temperatures.

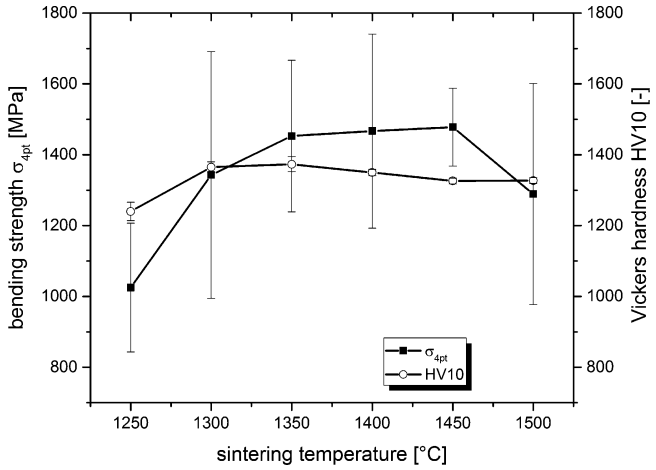

Fig. 5: Hardness HV10 and 4-pt bending strength σ_{4pt} of Y-TZP vs. sintering temperature.

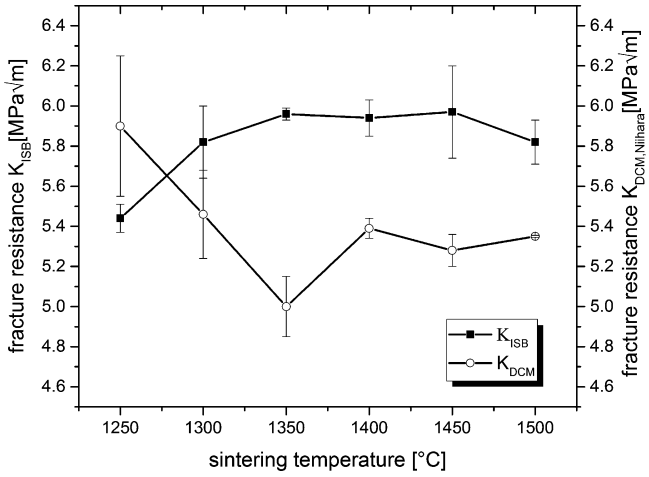

Fig. 6: Fracture resistance K_{ISB} and $K_{DCM,Niihara}$ of Y-TZP vs. sintering temperature.

(4) Mechanical properties

Fig. 5 shows the hardness and 4-pt bending strength of the materials. The Vickers hardness rises from 1300 HV10 at 1250 °C to 1400 HV10 at 1300 °C sintering temperature and stays almost constant at this level up to the highest sintering temperature. Bending strength increases from 1000 MPa at 1250 °C to 1450 MPa at 1350 °C then stays constant up to 1450 °C sintering temperature. At 1500 °C, a decrease in strength to 1270 MPa can be observed. Materials sintered at temperatures below and above the 1350 °C – 1450 °C range show a high scattering of strength values. Young's modulus E = 208 – 211 ± 5 GPa is almost constant irrespective of sintering temperature (not shown here). Poisson's ratio ν was 0.31 in all cases. The fracture resistance values determined by means of direct crack length measurement K_{DCM} and by ISB method K_{ISB} depending on sintering temperature of Y-TZP are shown in Fig. 6. While the K_{DCM} values show an initial decline with rising sintering temperature and a moderate rise beyond 1350 °C, the K_{ISB} values seem much more reliable. K_{DCM} may be strongly affected by the machining process inducing different states of residual stress in the region close to the surface. K_{ISB} values increase from 5.4 MPa√m at 1250 °C to a plateau toughness of ~ 6 MPa√m at 1300 – 1450 °C, toughness at 1500 °C slightly declines, which is surprising in respect of the higher transformability and the effect of grain size on fracture resistance. Fracture toughness data derived from stable indentation crack growth in bending SIGB can provide further information: the fracture resistance at infinite crack length $K_{IC,\,SIGB}$, resistance to subcritical crack growth K_{IO} and the R-curve-dependent part of the fracture resistance $K_{app,0}$ were determined. Fig. 7 shows two examples of SIGB plots for materials sintered at 1300 °C and 1500 °C. During indentation the crack driving stress intensity equals the toughness of the material, therefore after lifting the indenter, the indent stores a negative stress intensity K_{res}. During the bending test the crack having a length c will grow if the applied stress intensity K_{app} exceeds the value $K_{app,0}$ corresponding to the negative value of this stored stress intensity [25]. The onset of crack growth

is visible as a kink in the curve. Above $K_{app,0}$ cracks grow with rising stress σ and $\Psi\sigma\sqrt{c}$ rises linearly with declining $Pc^{-1.5}$. The slope χ is the residual stress coefficient (Ψ = 1.27 is a geometry factor). Fig. 7 shows that this relation applies to the sample sintered at 1300 °C. The curve of the material sintered at 1500 °C does not show a constant slope χ. χ grows with increasing crack length, thus the extrapolation to infinite crack length to obtain $K_{IC,\,SIGB}$ as the intercept with the ordinate does not seem acceptable and is prone to deliver exaggerated values of fracture resistance [31]. The methodology according to Dransmann *et al.* for the calculation of K_{I0} requires subtraction of the stress intensity $K_{app,0}$ at the kink from the extrapolated ordinate intercept ($K_{I0} = K_{IC,SIGB} - K_{app,0}$). Fig. 8 shows the results of this calculation. However, owing to the reasons discussed before, the authors would favor a conservative approach using K_{ISB} instead of $K_{IC,SIGB}$ to perform this calculation. $K_{IO,\,ISB}$ after an initial rise from 1250 °C to 1300 °C shows a constant value of 4.2 ± 0.1 MPa√m. This value is 1.4 MPa√m higher than values already reported determined by Chevalier *et al.* for 3Y-TZP in doube torsion tests and own results on coprecipitated hot-pressed 3Y-TZP (Tosoh TZ-3YSE sintered at 1450 °C/2 h) in SIGB [23].

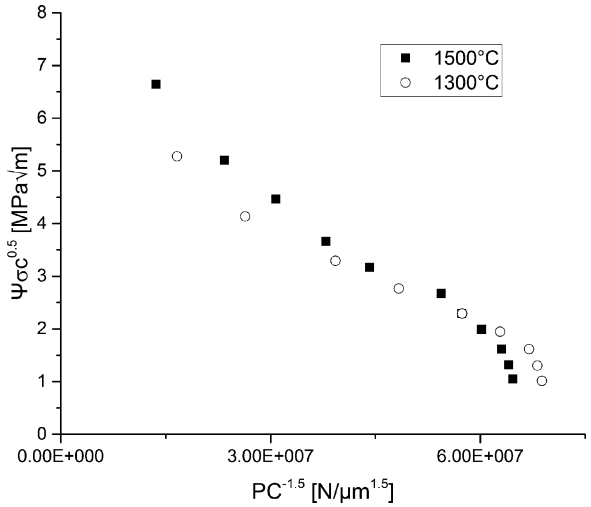

Fig. 7: Crack extension curves of stable indentation crack growth in bending SIGB experiments for samples sintered at 1300 °C and 1500 °C.

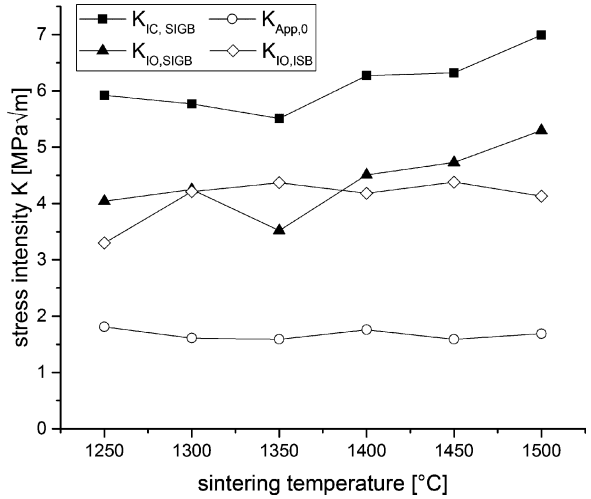

Fig. 8: Resistance to subcritical crack growth K_{IO}, R-curve-dependent part of fracture resistance $K_{App,0}$ and fracture resistance $K_{IC,SIGB}$ of Y-TZP vs. sintering temperature.

(5) Low-temperature degradation

Fig. 9 shows the surfaces of 3YTZP aged for different times at 134 °C in an accelerated autoclave test. The topography changes were visualized by means of differential interference contrast DIC. After 1 h at 134 °C, the transformation is restricted to the polishing-induced grooves. After 3 h, transformation lift-up can be detected, the lift-up zones are rough and located around circular regions. These circular regions with diameters ranging from 20 – 100 μm have smooth surfaces. Ageing clearly proceeds in the regions between these circular regions. Within the circular regions that are originally untransformed, it takes long ageing times of > 17 h until the formation of a corrugated surface indicates the onset of ageing. Cross-cut sections (Fig. 10) reveal that ageing proceeds at different speed in different regions while at 100 h the monoclinic layer in the center has a thickness of 13 – 14 μm, the layer thickness on the right side of the sample is much lower (~ 7 μm). As expected from the microscopy images (Fig. 9), the surface properties roughness R_z and waviness W_t determined by means of tactile measurement are strongly affected by ageing (Fig. 11). R_z values of unaged samples are initially ~ 20 nm, roughness starts to increase after an initial induction period of 10 h/134 °C (~ 12 vol% monoclinic), then a linear increase in roughness to 120 nm is observed up to 30 h (~ 60 vol% monoclinic). Beyond this point, roughness rises exponentially. Waviness W_t shows a slightly different trend, initial values of ~ 70 – 80 nm are preserved up to 10 h/134 °C, a plateau value of W_t ~ 100 nm extends to 30 h (~ 60 vol%) monoclinic. Then an increase to W_t ~ 400 nm at 100 h/134 °C follows. The plot of the monoclinic content at the surface of autoclave-aged samples $V_{m,\,aged}$ vs. ageing time shows the typical sigmoidal curve with the onset of fast ageing at 10 h which corresponds to the change in surface properties (not shown). According to the study by Chevalier *et al.* [13], the sigmoidal curve of LTD processes can be described by a nucleation and growth model of the following law: $V_{m,\,aged} = 1\text{-}\exp(b \cdot t)^n$ with $V_{m,\,aged}$ the monoclinic content, t the time b the rate constant and n an exponent. The MAJ (Mehl-Avrami-Johnson) plot is a linearized representation to determine values n and b. The MAJ-plot (Fig. 12) of $\ln\ln(1/1\text{-}V_{m,\,aged})$ vs. ln(t/h) over all measured values shows an Avrami exponent n (slope) of 1.04 ± 0.07 and a rate constant ln(b) (intercept) of -4.0 ± 0.2. There seems to be a change of ageing mechanism at 10 h/134 °C (ln(t/h) = 2.3) as the two segments before and after that (indicated by dashed lines) show somewhat flatter slopes and different intercepts. For the segment at low ageing times 1 – 10 h/134 °C regression analysis shows values of ln(b) = -3.81 ± 0.07 and n = 0.79 ± 0.05, the segment at longer ageing times 17 – 100 h/134 °C has an intercept of ln(b) = -2.28 ± 0.11 and n = 0.62 ± 0.03. Keuper has shown that XRD may underestimate the thickness of transformed layers, if the thickness of the monoclinic layers exceeds the penetration depth of x-rays (~ 8 – 10 μm) and data have to be cautiously interpreted [29]. Therefore we tried to correlate XRD data to values measured directly from microscope images of cross-cut and polished sections.

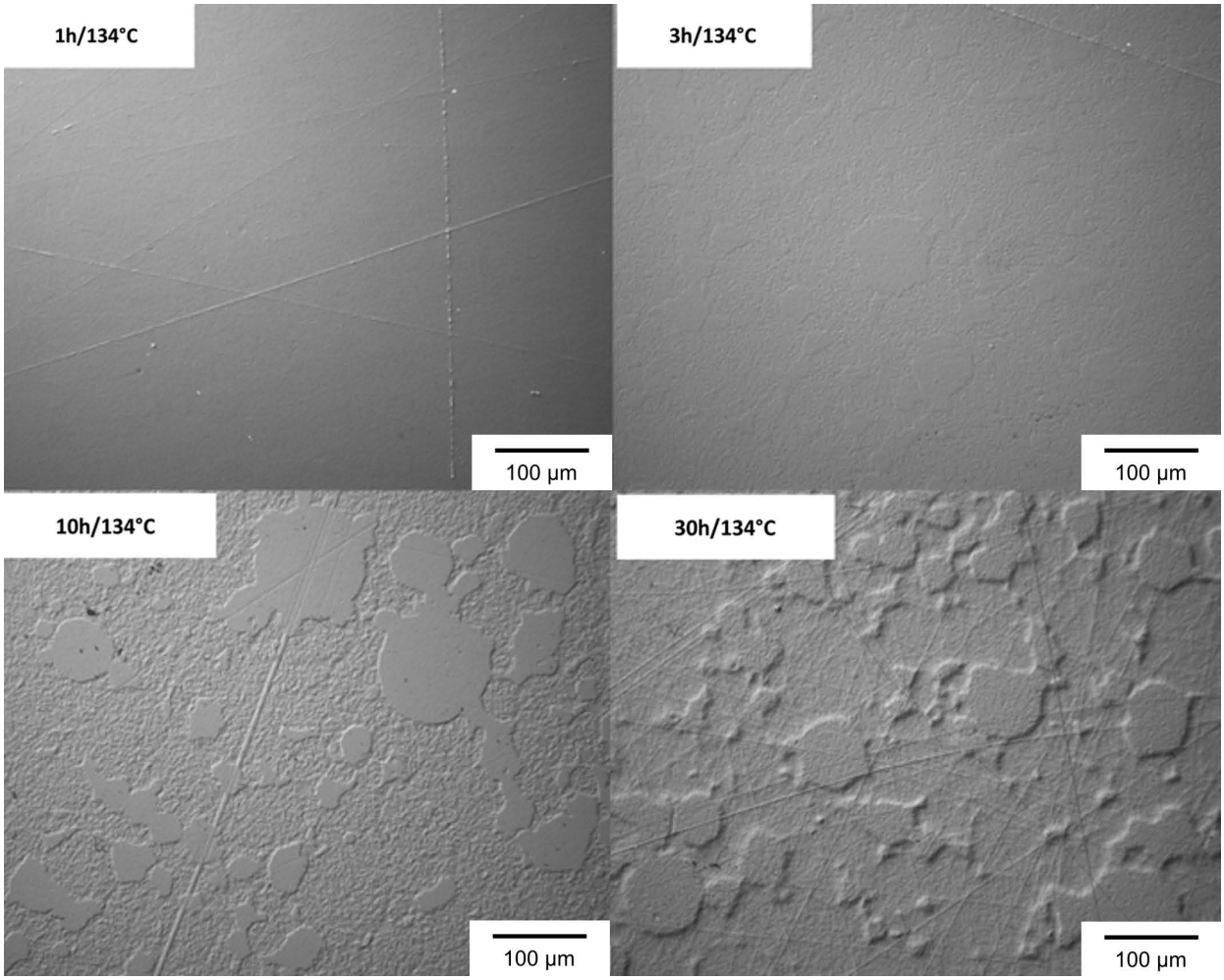

Fig. 9: Microscopy images made with differential interference contrast (DIC) to visualize the change in topography in autoclave-aged Y-TZP.

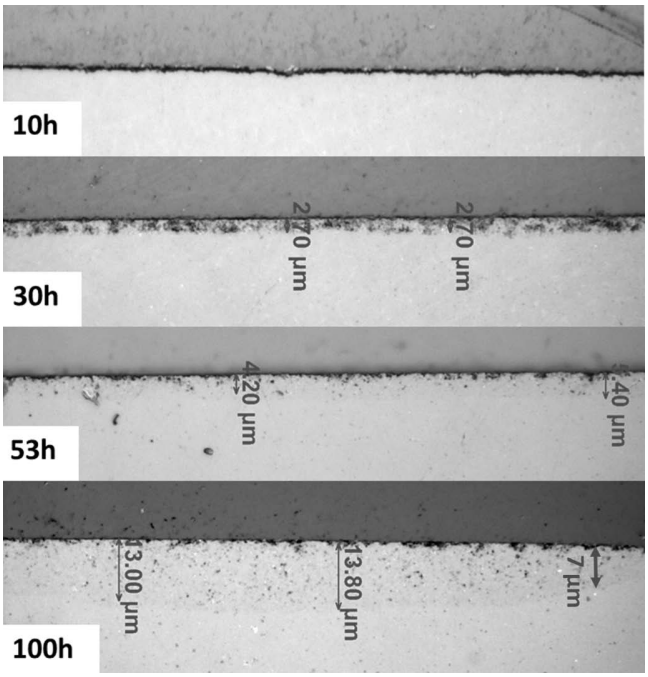

Fig. 10: Thickness of transformed layers in Y-TZP samples autoclave-aged at 134 °C for 10 h, 30 h, 53 h and 100 h.

Fig. 13 shows that the thickness of monoclinic scales measured by XRD and microscopy are quite close. The layer growth seems to follows a zero-order kinetic model ($dh/dt \sim k \cdot t^0$), only at very long ageing times and scale thickness > 10 µm the XRD underestimates the layer thickness owing to the limited depth of X-ray absorption.

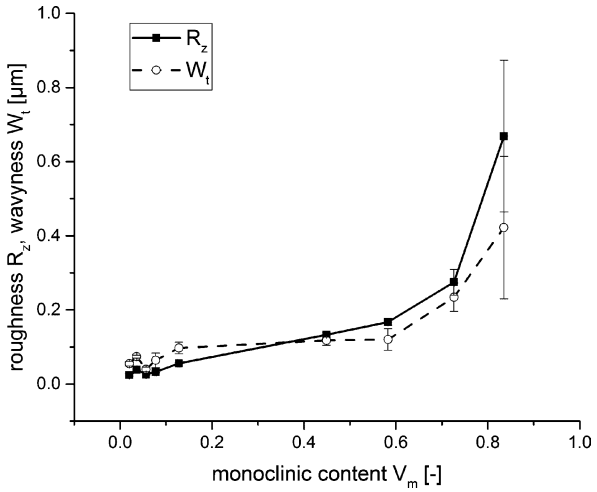

Fig. 11: Surface roughness R_z and waviness W_t of Y-TZP vs. ageing time at 134 °C.

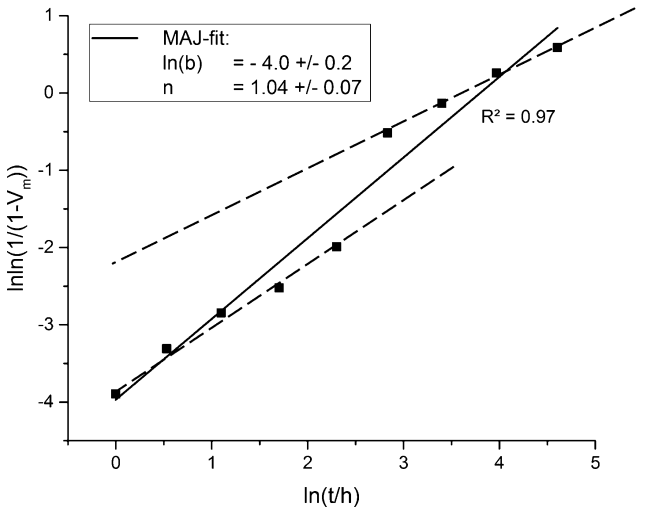

Fig. 12: Mehl-Avrami-Johnson plot of ageing kinetics, ordinate intercept shows rate constant ln(b), slope shows Avrami exponent n. Continuous line shows regression over all measured data. Dashed lines indicate different ageing kinetics in subsections.

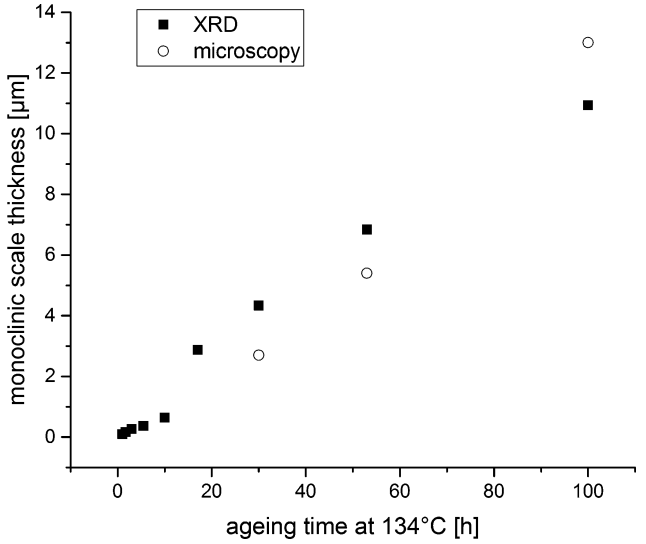

Fig. 13: Thickness of transformed layers in aged Y-TZP, comparison of measurements by XRD and microscopy.

IV. Discussion

The starting Y-TZP powder manufactured by means of emulsion detonation synthesis EDS contains a high amount of monoclinic, which implies that zirconia and yttria do not alloy intimately enough during the detonation synthesis process to form a solid solution. To a certain extent the tetragonal fraction may also be formed owing to small crystallite sizes and quenching of the high-temperature composition as has been observed for unstabilized zirconia nanopowder fabricated by Evonik by means of flame pyrolysis [26]. Hot-pressed 3Y-TZP materials exhibit high strength and hardness which are within the typical range of high-quality alumina-doped 3Y-TZP materials. Fracture resistance K_{ISB} (6 MPa √m) and resistance to subcritical crack K_{IO} (4.2 MPa√m) growth are higher than can be expected for coprecipitated 3Y-TZP (K_{IC} = 5 MPa√m, K_{IO} = 2.8 MPa√m [26]) but do not reach the high values found in materials prepared from stabilizer-coated powders (K_{IC} = 7 – 9 MPa√m, K_{IO} = 5.5 MPa√m [9, 30]). Y-TZP materials sintered at low temperatures (< 1350 °C) still contain some monoclinic. Transformability is relatively low considering the level of fracture resistance measured. As other toughening mechanisms than transformation toughening were not detected (strength is too high for microcrack toughening), the material probably has a slightly higher intrinsic fracture resistance than typical for 3Y-TZP [33].

Two ageing regimes were detected. The ageing resistance of the materials is high at moderate ageing times of 10 h/134 °C which corresponds to 30 – 40 years *in vivo* (which covers the lifetime of a dental implant). Chevalier *et al.* reported ln(b) values of -2.5 for 3Y-TZP, studies by the authors have found values for 2.5Y-TZP made from yttria-coated powder in the range of ln(b) = -4 [9, 13]. It can be assumed that the kinetics are similar to conventional Y-TZP at ageing times > 10 h (ln(b) ~ -2.7) while at ageing times < 10 h similarly high values (ln(b) = - 4.5) are found as for coated Y-TZP. The zero-order growth law of the LTD induced monoclinic layer as reported by Keuper and Kern can be fully confirmed at least for prolonged ageing times [32, 9].

The Y-TZP material made from EDS powder thus appears as a hybrid between Y-TZP made from coprecipitated and coated materials. It shows identical or improved mechanical and ageing properties compared to the state-of-the art coprecipitated material (particularly the relatively high fracture resistance at small grain size is difficult to achieve using coprecipitated 3Y-TZP) [5]. The values of Y-TZP made from stabilizer- coated powders (which are commercially unavailable) are exceeded as far as strength and hardness are concerned [6, 9, 30]. Fracture resistance, resistance to subcritical crack growth and ageing resistance are distinctly lower.

Some observations yet remain unexplained by the experiments carried out. The structure of aged surfaces with circular regions remaining unaffected by ageing for a considerable time suggest some inhomogeneity already present in the granulated starting powder and preserved in the sintered material. The size of the circular regions (Fig. 9) is in the range of 50 – 100 µm which coincides with the range of the powder granules. As the powder was used as-received without homogenization by milling, it may be that the detonation synthesis process leads to asymmetric deposition of stabilizer in individual granules. As differences in grain size were not observed, regions remaining untransformed may either contain more stabilizer or the stabilizer distribution is inhomogeneous. This may lead to features similar as in the case of Y-TZP material made from yttria-coated monoclinic powders or in blends of powders having low and high stabilizer contents. Burger and Piconi showed that 3Y-TZP materials made from coated starting powders showed almost no ageing despite high toughness and stress induced transformability [7]. Basu *et al.* showed that Y-TZP materials made from 3Y-TZP and monoclinic had higher fracture resistance than Y-TZP materials with the same stabilizer content introduced homogeneously by coprecipitation ("new mixing route" [34]). In principle both coating and "new mixing route" exploit the same effect. Monoclinic powders will take up yttria (no matter if from

their yttria coating or from nearby 3Y-TZP grains containing excess yttria) until their composition reaches the composition at the t/t+c phase boundary (~ 2.5 mol% at typical sintering temperature of ~ 1400 °C). Initially a stabilizer gradient will be formed, resulting in grains with a sufficiently stabilized shell and an understabilized and very transformable core. The difference is that in case of the "new mixing route", only a part of the grains show the gradient so that the additional toughening increment is relatively moderate. These issues will have to be studied in detail.

V. Summary

3Y-TZP ceramics were manufactured from a new starting powder made synthesized by means of EDS. Mechanical properties and resistance to LTD were comparable to or better than the state-of-the-art materials made from coprecipitated powders processed by hot pressing. The new type of powders has become commercially available and may be an interesting and affordable powder source for applications in mechanical engineering or biomedical sectors. As the bending strength reaches 1400 MPa and K_{IO}/K_{ISB} = 0.7 (if sintered at 1350 °C – 1450 °C), the materials should offer a superior fatigue strength of up to 1000 MPa compared to standard 3Y-TZP (~ 600 MPa). If the materials are sintered under oxidizing conditions, we may expect an even higher ageing resistance [35]. Based on the properties determined the materials would fulfill the requirements of the dental standard with regard to strength, grain size and resistance to LTD. Some features of the powder are not fully understood yet and will require further investigations.

Acknowledgements

The authors would like to thank the powder producer for supplying a test batch of powder, Felicitas Predel for making SEM images and Willi Schwan for assistance in sample preparation and microscopy.

References:

[1] Hannink, R.H.J., Kelly, P.M., Muddle, B.C.: Transformation toughening in zirconia-containing ceramics, *J. Am. Ceram. Soc.*, **83**, 461 – 87, (2000).

[2] Kelly P.M., Rose, L.R.F.: The martensitic transformation of ceramics – its role in transformation toughening, *Prog. Mater. Sci.*, **67**, 463 – 557, (2002).

[3] Li, P., Chen, I.W., Penner-Hahn, J.: Effect of dopants on zirconia stabilization – an x-ray absorption study: I, trivalent dopants, *J. Am. Ceram. Soc.*, **77**, 118 – 28, (1994).

[4] Chen, M., Hallstedt, B., Gauckler, L.: Thermodynamic modeling of the ZrO_2-$YO_{1.5}$ system, *Solid State Ionics*, **170**, 255 – 274, (2004).

[5] Ruiz, L., Readey, M.J.: Effect of heat treatment on grain size, phase assemblage and mechanical properties of 3Y-TZP, *J. Am. Ceram. Soc.*, **79**, 2331 – 2340, (1996).

[6] Singh, R., Gill, C., Lawson, S., Dransfield, G.P.: Sintering, microstructure and mechanical properties of commercial Y-TZPs, *J. Mater. Sci.*, **31**, 6055 – 62, (1996).

[7] Burger, W., Richter, H.G., Picconi, C., Vatteroni, R., Cittadini, A., Boccalari, M.: New Y-TZP powders for medical grade zirconia, *J. Mater. Sci. – Mater. M*, **8**, 113 – 8, (1997).

[8] Ohnishi, H., Naka, H., Sekino, T., Ikuhara, Y., Niihara, K.: Mechanical properties of 2.0 – 3.5 mol% Y_2O_3-stabilized zirconia polycrystals fabricated by the solid phase mixing and sintering method, *J. Ceram. Soc. Jpn.*,**116**, 1270 – 1277, (2008).

[9] Kern, F.: Mechanical properties and low temperature degradation resistance of 2.5Y-TZP – alumina composites, *Materialy Ceramiczne/Ceramic Materials*, **65**, 258 – 266, (2013).

[10] Schubert, H., Frey, F.: Stability of Y-TZP during hydrothermal treatment: neutron experiments and stability considerations, *J. Eur. Ceram. Soc.*, **25**, 1597 – 602, (2005).

[11] Chevalier, J., Gremillard, L., Virkar, A.V., Clarke, D.R.: The tetragonal-monoclinic transformation in zirconia: lessons learned and future trends, *J. Am. Ceram. Soc.*, **92**, 1901 – 1920, (2009).

[12] Chevalier, J., Gremillard, L. Deville, S.: Low temperature degradation of zirconia and implications for biomedical implants, *Annu. Rev. Mater. Res.*, **37**, 1 – 32, (2007).

[13] Chevalier, J., Drouin, J.M., Cales, B.: Low-temperature aging of Y-TZP ceramics, *J. Am. Ceram. Soc.*, **82**, 2150 – 54, (1999).

[14] Gremillard, L., Chevalier, J., Epicier, T., Deville, S., Fantozzi, G.: Modeling the aging kinetics of zirconia ceramics, *J. Eur. Ceram. Soc.*, **24**, 3483 – 3489, (2004).

[15] Deville, S., Gremillard, L., Chevalier, J., Fantozzi, G.: A critical comparison of methods for the determination of the aging sensitivity in biomedical grade yttria-stabilized zirconia, *J. Biomed. Mater. Res. B*, **72**, 239 – 245, (2005).

[16] Neves, N., Barros, R., Antunes, E., Calado, J., Fortunato, E., Martins, R., Ferreira, I.: Aluminum doped zinc oxide sputtering targets obtained from nanostructured powders: processing and application, *J. Eur. Ceram. Soc.*, **32**, 4381 – 4391, (2012).

[17] Neves, N., Lagoa, L., Calado, J., Rego, A.M.B., Fortunato, E., Martins, R., Ferreira, I.: Al-doped ZnO nanostructured powders by emulsion detonation synthesis – improving materials for high quality sputtering targets manufacturing, *J. Eur. Ceram. Soc.*, **34**, 2325 – 38, (2014).

[18] Calado, J.: Ceramic powder production with emulsion detonation synthesis, *cfi/Ber. DKG*, **93**, [4 – 5], E32 – E34, (2016).

[19] Calado, J., Innovation through detonation: designing improved ceramic composites, Ceramic Industry (online), March 1 (2016)

[20] Calado, J., Dos Santos, E.: Nanocrystaline spherical ceramic oxides, process for the synthesis and use thereof, US patent 9249020 B2.

[21] Toraya, H., Yoshimura, M., Somiya, S.: Calibration curve for quantitative analysis of the monoclinic-tetragonal ZrO_2 system by X-ray diffraction, *J. Am. Ceram. Soc.*, **67**, C119 – C121, (1984).

[22] Patterson, A.L.: The scherrer formula for X-Ray particle size determination, *Phys. Rev.*, **56**, 978 – 82, (1939).

[23] Chantikul, P., Anstis, G.R., Lawn, B.R., Marshall, D.B.: A critical evaluation of indentation techniques for measuring fracture Toughness: II, strength method, *J. Am. Ceram. Soc.*, **64**, 539 – 543, (1981).

[24] Niihara, K.: A fracture mechanics analysis of indentation-induced palmqvist crack in ceramics, *J. Mater. Sci. Lett.*, **2**, 221 – 223, (1983).

[25] Dransmann, G.W., Steinbrech, R.W., Pajares, A., Guiberteau, F., Dominguez-Rodriguez, A., Heuer, A.: Indentation studies on Y_2O_3-Stabilized ZrO_2: II, toughness determination from stable growth of Indentation-Induced cracks, *J. Am. Ceram. Soc.*, **77**, 1194 – 1201, (1994).

[26] Benzaid, R., Chevalier, J., Saâdaoui, M., Fantozzi, G., Nawa, M., Diaz, L.A., Torrecillas, R.: Fracture toughness, strength and slow crack growth in a ceria stabilized zirconia-alumina nanocomposite for medical applications, *Biomaterials*, **29**, 3636 – 41, (2008).

[27] Kosmac, T., Wagner, R., Claussen, N.: X-Ray determination of transformation depths in ceramics containing tetragonal ZrO_2, *J. Am. Ceram. Soc.*, **64**, [4], C72 – 3, (1981).

[28] McMeeking, R.M., Evans, A.G.: Mechanics of Transformation-Toughening in brittle materials, *J. Am. Ceram. Soc.*, **65**, [5], 242 – 46, (1982).

[29] Mendelson, M.I.: Grain size in polycrystalline ceramics, *J. Am. Ceram. Soc.*, **52**, 443 – 444, (1969).

[30] Kern, F.: 2.5Y-TZP from yttria-coated pyrogenic zirconia nanopowder, *J. Ceram. Sci. Tech.*, **1**, 21 – 26, (2010).

[31] Lube, T., Fett, T.: A threshold stress intensity factor at the onset of stable crack extension of knoop indentation cracks, *Eng. Fract. Mech.*, **71**, 2263 – 69, (2004).

[32] Keuper, M., Eder, K., Berthold, C., Nickel, K.G.: Direct evidence for continuous linear kinetics in the low-temperature degradation of Y-TZP, *Acta Biomater.*, **9**, 4826 – 35, (2013).

[33] Swain, M.V., Rose, L.R.F.: Strength limitations of transformation-toughened zirconia alloys, *J. Am. Ceram. Soc.*, **69**, 511 – 518, (1986).

[34] Basu, B., Vleughels, J., Van der Biest, O.: Toughness tailoring of yttria-doped zirconia ceramics, *Mat. Sci. Eng. A*, **380**, 215 – 221, (2004).

[35] Bartholomé, J.F., Montera, I., Diaz, M., Lopez-Esteban, S., Moya J.S.: Accelerated aging in 3-mol%-yttria-stabilized tetragonal zirconia ceramics sintered in reducing conditions, *J. Am. Ceram. Soc.*, **87**, 2282 – 2285, (2004).